# Photon-number distributions of twin beams generated in spontaneous parametric down-conversion and measured by an intensified CCD camera

Jan Peřina Jr.,* Martin Hamar, and Václav Michálek
*Institute of Physics of Academy of Sciences of the Czech Republic, Joint Laboratory of Optics of Palacký University and Institute of Physics of Academy of Sciences of the Czech Republic, 17. listopadu 12, 772 07 Olomouc, Czech Republic*

Ondřej Haderka
*RCPTM, Joint Laboratory of Optics of Palacký University and Institute of Physics of Academy of Sciences of the Czech Republic, Faculty of Science, Palacký University, 17. listopadu 12, 771 46 Olomouc, Czech Republic*

(Received 27 September 2011; published 14 February 2012)

The measurement of photon-number statistics of fields composed of photon pairs, generated in spontaneous parametric down-conversion and detected by an intensified charge-coupled device (iCCD) camera, is described. Final quantum detection efficiencies, electronic noises, finite numbers of detector pixels, transverse intensity spatial profiles of the detected beams, as well as losses of single photons from a pair are taken into account in a developed general theory of photon-number detection. The measured data provided by an iCCD camera with single-photon detection sensitivity are analyzed along the developed theory. Joint signal-idler photon-number distributions are recovered using the reconstruction method based on the principle of maximum likelihood. The range of applicability of the method is discussed. The reconstructed joint signal-idler photon-number distribution is compared with that obtained by a method that uses superposition of signal and noise and minimizes photoelectron entropy. Statistics of the reconstructed fields are identified to be multimode Gaussian. Elements of the measured as well as the reconstructed joint signal-idler photon-number distributions violate classical inequalities. Sub-shot-noise correlations in the difference of the signal and idler photon numbers as well as partial suppression of odd elements in the distribution of the sum of signal and idler photon numbers are observed.

DOI: 10.1103/PhysRevA.85.023816 PACS number(s): 42.65.Lm, 42.50.Ar

## I. INTRODUCTION

Light generated in the process of spontaneous parametric down-conversion (SPDC) is emitted in photon pairs [1]. Photons comprising one photon pair are strongly quantum correlated (entangled). Entanglement of photons in a pair has been used in many experiments that have provided a deep insight into the laws of quantum mechanics [2,3]. Among others, the measured violation of Bell's inequalities ruled out neoclassical local hidden-variable theories. Photon pairs have also found their way into practical applications, e.g., in quantum cryptography [4], in the measurement of ultrashort time delays, or in absolute measurements of detection quantum efficiencies [5,6]. These experiments utilize photon fields that contain only one photon pair in a measured time window with a high probability.

There have been experiments [teleportation, measurement of Greenberger-Horne-Zeilinger correlations, etc.] measuring triple and quadruple coincidence counts caused by fields containing two photon pairs in a time window given by an ultrashort pump pulse. However, states used for such experiments contain a very low fraction of states with two photon pairs in comparison with the fraction belonging to the state with one photon pair and the vacuum state. The reason is to eliminate the influence of three and more-than-three photon-pair states to the considered experimental setups. Measurements done in such setups have to be conditional and they require long data-acquisition times.

The use of more powerful pump pulses as well as the development of materials with higher values of $\chi^{(2)}$ susceptibilities have opened the way to generate fields containing many photon pairs originating in one pump pulse. For such fields, a joint signal-idler photon-number distribution is the main characteristic that determines the experimental results utilizing these fields. Determination of photon-pair statistics is important also for weak cw fields provided that they are detected in long-time-detection windows [7]. In this case photon-pair statistics have been identified to be Poissonian after eliminating dead-time detection effects [7].

Returning back to more intense fields, recent experiments ([8–15] and references therein) are even able to provide experimental joint signal-idler photoelectron distributions of twin beams containing up to several thousands of photon pairs. As for detectors, weaker fields containing up to ten photons can be measured by special single-photon avalanche detectors (VLPC) [16], hybrid photomultipliers [17,18], superconducting bolometers [19], or time-multiplexed fiber-optics detection loops [20–25]. Intensified charge-coupled device (CCD) cameras [11,26,27] can in principle capture states with hundreds of photons. Ultrasensitive photodiodes with their linear response and very low level of noise are suitable for the detection of states with hundreds or, even better, thousands of photons. A special method utilizing precisely attenuated beams has also been suggested and developed [28,29]. It allows to resolve photon numbers even in the measurement based on single-photon-sensitive avalanche photodiodes. We note that also the well-known homodyne detection has been found useful in the determination of intensity correlations of twin beams [30,31].

*perinaj@prfnw.upol.cz

 

All these approaches give experimental photoelectron distributions obtained by detectors with finite quantum detection efficiencies. While silicon *p-i-n* photodiodes or back-illuminated CCD cameras can offer detection efficiencies close to unity, their internal noise prevents their use in the single-photon regime. On the other hand, detectors with large internal gain, such as intensified CCD (iCCD) cameras, electron-multiplying CCD (EMCCD) cameras, or avalanche photodetectors, allow single-photon sensitivity or even photon-number resolution by effectively decreasing their noise. A price for this sensitivity is paid, however, in the form of lower quantum detection efficiencies. The iCCD cameras are a good trade-off in this respect. Their level of noise is low, but not negligible. On the other hand, quantum detection efficiencies around 20% are sufficient enough to profit from their low level of noise.

Once we know the quantum detection efficiency and the level of noise, we can reconstruct the field in front of a detector. The usual and physically motivated approach is based on the assumption of the character of the reconstructed field. Working with photon pairs, we can naturally assume that the reconstructed field is composed of a certain number of independent modes containing photon pairs and small additional noise in the form of single photons. Using this picture, a multimode theory of signal and noise tailored especially for paired fields can be applied (see [32,33] for the spontaneous process and [34–36] for the stimulated process). It can be accompanied by the principle of minimum entropy to get the reconstructed field. As an alternative, one may rely on a mathematically based method that uses the maximum-likelihood principle. In the framework of this method, the reconstructed field is reached as a steady point accessible by an iteration procedure. As a final step in the characterization of the fields, joint signal-idler quasi-distributions of integrated intensities may be reached using the reconstructed joint signal-idler photon-number distributions [12,37].

Here, we pay attention to the determination of a joint signal-idler photon-number distribution beyond a nonlinear crystal using an iCCD camera as a tool to resolve photon numbers. The method of maximum likelihood is applied. It allows to deal with even more difficult experimental conditions such as those reached when more than one photon can be registered in a single pixel. Transformation matrices describing details of the detection process and being an important ingredient of the iteration procedure are derived under several conditions. The reconstructed fields are compared with those obtained by the method of superposition of signal and noise.

The paper is organized as follows. Section II contains a general model describing a photon-number-resolving detection device. Section III is devoted to the description of photon-number-resolving detection by an iCCD camera under real experimental conditions. The role of inhomogeneous transverse profiles of the detected fields is discussed in Sec. IV. In Sec. V, the iteration procedure of the maximum-likelihood method is explained and used to recover joint signal-idler photon-number distributions. Section V A is devoted to nonclassical characteristics of the emitted fields. Statistics of the fields are discussed in Sec. V B, in which the problem of reconstruction of more intense fields is also addressed. Comparison of the reconstructed fields obtained by the maximum-likelihood method and the method of superposition of signal and noise is provided in Sec. VI. Section VII brings conclusions. The formula for an effective quantum detection efficiency is derived in Appendix.

## II. PROBABILITIES OF MULTIPHOTON-COINCIDENCE COUNTS IN AN ARRAY OF SINGLE-PHOTON DETECTORS

The measurement of joint signal-idler photon-number distribution can be in general described using the scheme shown in Fig. 1 [38–40]. Photon pairs occurring in the output plane of a nonlinear crystal propagate toward photon-number-resolving detection devices placed in the paths of the signal and idler fields. One or both photons from a pair may be lost before they reach their detection devices. Geometric filtering (one photon from a pair is not steered to the detector area), reflections on optical elements in the experimental setup, or absorption of a photon along its path to a detection device represent possible reasons. We describe this effect by two beam splitters, $\mathrm{BS}_S$ and $\mathrm{BS}_I$ [41], placed in the signal and idler field paths, respectively. We model a photon-number-resolving detection device as a multiport $1 \times N$ [42] followed by $N$ single-photon detectors. This description holds also in the special case when an intensified CCD camera is used [26]. We note that detectors able to resolve directly photon numbers to some extent have been constructed [16,19,43]. From a practical viewpoint, also detectors using time multiplexing (reached, e.g., in fiber optics) and one or two single-photon detectors are promising [21,22,25]. Photon-number-resolving detection

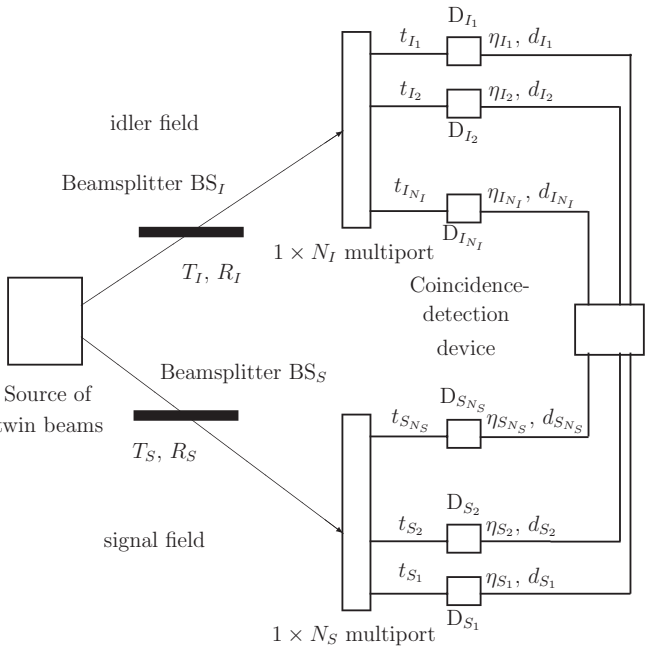


FIG. 1. Scheme of the considered model. Photon pairs are generated in a nonlinear crystal. Virtual beam splitters $\mathrm{BS}_S$ and $\mathrm{BS}_I$ describe possible losses of one or both photons from a pair before they are detected. Signal (idler) photons propagate through a $1 \times N_S$ ($1 \times N_I$) multiport and are detected by single-photon detectors $\mathrm{D}_{S_1}, \mathrm{D}_{S_2}, \ldots, \mathrm{D}_{S_{N_S}}$ ($\mathrm{D}_{I_1}, \mathrm{D}_{I_2}, \ldots, \mathrm{D}_{I_{N_I}}$). Signals from the detectors are registered in a coincidence-detection device.

in all these devices can be described in the framework of the presented general model.

We assume that the signal and idler fields in the output plane of the nonlinear crystal are described by the following statistical operator $\hat{\rho}_{SI}$ written in the Fock basis:

$$\hat{\rho}_{SI} = \sum_{n_S=0}^{\infty}\sum_{n_I=0}^{\infty} p(n_S,n_I)|n_S\rangle_{SS}\langle n_S| \otimes |n_I\rangle_{II}\langle n_I|; \quad (1)$$

the symbol $p(n_S,n_I)$ stands for the joint signal-idler photon-number distribution.

The statistical operator $\hat{\rho}_{SI}^{D}$ appropriate for the signal and idler fields in front of the detection devices can be expressed as:

$$\hat{\rho}_{SI}^{D} = \sum_{n_S=0}^{\infty}\sum_{n_I=0}^{\infty} p(n_S,n_I)\sum_{l_S=0}^{n_S}\binom{n_S}{l_S} T_S^{l_S} R_S^{n_S-l_S}|l_S\rangle_{SS}\langle l_S| \times \sum_{l_I=0}^{n_I}\binom{n_I}{l_I} T_I^{l_I} R_I^{n_I-l_I}|l_I\rangle_{II}\langle l_I|. \quad (2)$$

The symbols $R_S$ and $R_I$ ($T_S$ and $T_I$) denote intensity reflectivities (transmissivities) of the beam splitters in the corresponding path.

We assume a multiport $1\times N_S$ ($1\times N_I$) followed by $N_S$ ($N_I$) single-photon detectors with quantum efficiencies $\eta_{S_j}$ ($\eta_{I_j}$) and dark-count rates $d_{S_j}$ ($d_{I_j}$) in the signal (idler) path. Detection of a photon in the $k$th detector is described by the following detection operator $\hat{D}_{i_k}$ [38]:

$$\hat{D}_{i_k} = \sum_{n=0}^{\infty}\left\{\left[1-\left(1-\eta_{i_k}\right)^n\right] + d_{i_k}\left(1-\eta_{i_k}\right)^n\right\}|n\rangle_{kk}\langle n|, \quad i = S,I. \quad (3)$$

On the other hand, detection operator $\hat{D}_{i_k}^{\mathrm{no}}$ corresponds to the case when no detection has occurred:

$$\hat{D}_{i_k}^{\mathrm{no}} = 1 - \hat{D}_{i_k}. \quad (4)$$

The effect of "splitting" photons in the signal field in a $1\times N_S$ multiport can be described by the relation $\hat{a}_S = \sum_{j=1}^{N_S} t_{S_j}\hat{a}_{S_j}$, where $\hat{a}_S$ is the annihilation operator in the signal field entering the multiport, whereas the annihilation operator $\hat{a}_{S_j}$ describes a field at the $i$th multiport output. The symbol $t_{S_j}$ stands for an amplitude transmissivity of a photon from the input to the $j$th output. The $1\times N_I$ multiport in the idler-field path is described similarly and the symbol $t_{I_j}$ then refers to an amplitude transmissivity of a photon from the input to the $j$th multiport output.

The probability $C_{S^D,I^D}$ that given $c_S$ detectors in the signal field and given $c_I$ detectors in the idler field detect a photon, whereas the rest of the detectors do not register a photon, is determined as the quantum mean value:

$$C_{S^D,I^D} = \mathrm{Tr}_{SI}\left\{\hat{\rho}_{SI}^{D}\prod_{a\in S^D}\hat{D}_a\prod_{b\in S\setminus S^D}\hat{D}_b^{\mathrm{no}}\prod_{c\in I^D}\hat{D}_c\prod_{d\in I\setminus I^D}\hat{D}_d^{\mathrm{no}}\right\}. \quad (5)$$

The symbol $S$ ($I$) denotes the set of all signal-field (idler-field) detectors $S=\{S_1,\ldots,S_{N_S}\}$ ($I=\{I_1,\ldots,I_{N_I}\}$). The set $S^D$ ($I^D$) contains signal-field (idler-field) detectors that have registered a photon. Tr stands for an operator trace.

Using the statistical operator $\hat{\rho}_{SI}^{D}$ given in Eq. (2), the probability $C_{S^D,I^D}$ of a multicoincidence count defined in Eq. (5) is obtained in the form

$$\begin{aligned}
C_{S^D,I^D} &= \sum_{n_S=0}^{\infty}\sum_{n_I=0}^{\infty} p(n_S,n_I)K_{S,S^D}(n_S)K_{I,I^D}(n_I),\\
K_{S,S^D}(n_S) &= (-1)^{c_S}\left[\prod_{b\in S}(1-d_b)\right]\left[T_S\left(\sum_{c\in S}|t_c|^2(1-\eta_c)\right)+R_S\right]^{n_S}\\
&\quad+\frac{(-1)^{c_S-1}}{1!}\sum_{a\in S^D}\left[\prod_{b\in S\setminus\{a\}}(1-d_b)\right]\left[T_S\left(|t_a|^2\eta_a+\sum_{c\in S\setminus\{a\}}|t_c|^2(1-\eta_c)\right)+R_S\right]^{n_S}+\cdots\\
&\quad+\left[\prod_{b\in S\setminus S^D}(1-d_b)\right]\left[T_S\left(\sum_{c\in S^D}|t_c|^2+\sum_{c\in S\setminus S^D}|t_c|^2(1-\eta_c)\right)+R_S\right]^{n_S},\\
K_{I,I^D}(n_I) &= (-1)^{c_I}\left[\prod_{b\in I}(1-d_b)\right]\left[T_I\left(\sum_{c\in I}|t_c|^2(1-\eta_c)\right)+R_I\right]^{n_I}\\
&\quad+\frac{(-1)^{c_I-1}}{1!}\sum_{a\in I^D}\left[\prod_{b\in I\setminus\{a\}}(1-d_b)\right]\left[T_I\left(|t_a|^2\eta_a+\sum_{c\in I\setminus\{a\}}|t_c|^2(1-\eta_c)\right)+R_I\right]^{n_I}+\cdots\\
&\quad+\left[\prod_{b\in I\setminus I^D}(1-d_b)\right]\left[T_I\left(\sum_{c\in I^D}|t_c|^2+\sum_{c\in I\setminus I^D}|t_c|^2(1-\eta_c)\right)+R_I\right]^{n_I}.
\end{aligned} \quad (6)$$

We now consider two symmetric multiports ($t_{S_1} = t_{S_2} = \cdots = t_{S_{N_S}} = t_S = 1/\sqrt{N_S}$, $t_{I_1} = t_{I_2} = \cdots = t_{I_{N_I}} = t_I = 1/\sqrt{N_I}$) and detectors endowed with the same characteristics in the signal and idler fields ($\eta_{S_1} = \eta_{S_2} = \cdots = \eta_{S_{N_S}} = \eta_S$, $d_{S_1} = d_{S_2} = \cdots = d_{S_{N_S}} = d_S$, $\eta_{I_1} = \eta_{I_2} = \cdots = \eta_{I_{N_I}} = \eta_I$, $d_{I_1} = d_{I_2} = \cdots = d_{I_{N_I}} = d_I$). Then the probability $f^{N_S,N_I}(c_S,c_I)$ of having $c_S$ detections somewhere at $N_S$ signal detectors and $c_I$ detections somewhere at $N_I$ idler detectors can be expressed as

$$f^{N_S,N_I}(c_S,c_I) = \binom{N_S}{c_S}\binom{N_I}{c_I} C_{S^D,I^D}. \tag{7}$$

Using the expression for $C_{S^D,I^D}$ provided in Eq. (6) we arrive at the relation

$$f^{N_S,N_I}(c_S,c_I) = \sum_{n_S=0}^{\infty}\sum_{n_I=0}^{\infty} p(n_S,n_I) K^{S,N_S}(c_S,n_S) K^{I,N_I}(c_I,n_I), \tag{8}$$

where

$$K^{i,N_i}(c_i,n_i) = \binom{N_i}{c_i}(1-d_i)^{N_i}(1-\tau_i)^{n_i}(-1)^{c_i} \times \sum_{l=0}^{c_i}\binom{c_i}{l}\frac{(-1)^l}{(1-d_i)^l}\left(1+\frac{l}{N_i}\frac{\tau_i}{1-\tau_i}\right)^{n_i}, \quad i = S,I, \tag{9}$$

and where $\tau_i$ ($\tau_i = T_i\eta_i$) determines the probability that a photon is registered at some of the detectors.

If the number of photons detected by the camera is much lower than the number of pixels detecting the overall field with a non-negligible probability, the limits $N_S \to \infty$ and $N_I \to \infty$ are appropriate. When determining these limits, the overall noise levels $D_S$ and $D_I$ are kept constant ($D_S = N_S d_S$, $D_I = N_I d_I$). The coefficients $K$ defined in Eq. (9) then considerably simplify:

$$K^{i,\infty}(c_i,n_i) = \sum_{l=0}^{\min(c_i,n_i)}\binom{n_i}{l}(\tau_i)^l(1-\tau_i)^{n_i-l} \times \frac{D_i^{c_i-l}}{(c_i-l)!}\exp(-D_i), \quad i = S,I. \tag{10}$$

We note that the following relations have been used when deriving Eq. (10):

$$\sum_{k=0}^{N}\binom{N}{k}(-1)^k(\alpha+k)^{n-1} = 0,$$
$$N \geqslant n \geqslant 1, \quad 0^0 \equiv 1, \quad N,n \in N^+,$$
$$\sum_{k=0}^{N}\binom{N}{k}(-1)^k(\alpha+k)^N = (-1)^N N!,$$
$$N \geqslant 0, \quad 0^0 \equiv 1,$$

where $N^+$ denotes positive-integer numbers.

## III. PHOTON-NUMBER DETECTION UNDER REAL EXPERIMENTAL CONDITIONS

In our typical experiment (see Fig. 2) we define three regions of interest on the iCCD detection photocathode: one for collecting signal photons, one for counting idler photons, and one that serves for monitoring the dark noise in the experiment. To achieve higher data collection rates we use hardware binning of several pixels to a single macropixel. The signal and idler regions typically contain about one thousand macropixels that give information about photon detection. This means that a finite number of (macro)pixels may play an important role depending on the intensity of the impinging field, and the general form of the transfer matrix $K^{i,N_i}(c_i,n_i)$ in Eq. (9) should be preferably used. However, evaluation of a transfer matrix $K$ for larger numbers of photons, photoelectrons (registered photons), and (macro)pixels is difficult because a high extended precision in the evaluation of the sum occurring in Eq. (9) is required. For instance, if fields having up to 1000 photons are measured, from 200 to 300 significant decimal digits are needed in the evaluation of the sums in Eq. (9) under the conditions considered below. This is time demanding and that is why we present several alternative ways to handle the problem under specific conditions.

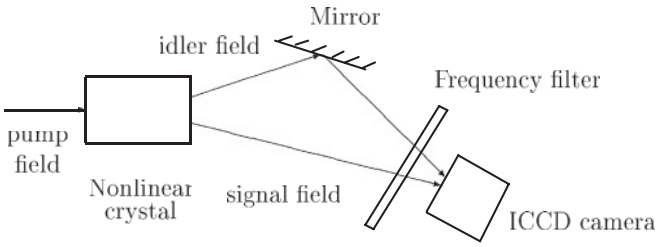


FIG. 2. Scheme of the setup for detection of photon pairs. Fields composed of typically tens or hundreds of photon pairs are generated in a nonlinear crystal. Idler photons are reflected on a mirror. Both signal and idler photons propagate through a frequency filter and are detected in an iCCD camera.

First, we rewrite the relation between the measured frequencies $f^{N_S,N_I}$ and the photon-number distribution $p$ in a general form:

$$f^{N_S,N_I}(c_S,c_I) = \sum_{n_S=0}^{\infty}\sum_{n_I=0}^{\infty} p(n_S,n_I) \times G^{S,N_S}(c_S,n_S) G^{I,N_I}(c_I,n_I), \tag{11}$$

where the general transformation matrices $G^{i,N_i}(c_i,n_i)$ for $i = S,I$ have been introduced.

In a real experimental setup, there are non-negligible losses (described by intensity transmissivities $T_S$ and $T_I$) before a field arrives to the photocathode of the iCCD camera. As a result the average number of photons in the input to the camera is lower compared to the average number of photons in the output plane of the crystal. This may make a numerical evaluation of the matrix $K^{i,N_i}$ in Eq. (9) faster due to lower dimensions of this matrix. In this case the transfer matrix $G^{i,N_i}(c_i,n_i)$ can be rewritten as a product of two matrices:

$$G^{i,N_i}(c_i,n_i) = \sum_{m=0}^{n_i} K^{i,N_i}(c_i,m) K_0(m,n_i). \tag{12}$$

The matrix $K_0$ introduced in Eq. (12) describes the Bernoulli distribution with transmissivity $T_i$:

$$K_0(m,n_i) = \binom{n_i}{m} T_i^m (1-T_i)^{n_i-m}. \tag{13}$$

Evaluation of the matrix $K^{i,N_i}$ using Eq. (9) is then done assuming $\tau_i = \eta_i$.

If numbers of photons in a detected field are too high, preventing the application of Eq. (9) (technical reasons in the evaluation), we can proceed as follows. The measured field first undergoes losses described by the intensity transmissivity $T_i$ before impinging on the camera. In the next step each photon present in the region of interest of the camera "registers" itself in one (macro)pixel. The probability $\gamma^{i,N_i}(m_2,m_1)$ that $m_1$ photons register in $m_2$ (macro)pixels, assuming the overall number of (macro)pixels to be $N_i$, is given by permutations with repetition:

$$\gamma^{i,N_i}(m_2,m_1) = \frac{\binom{N_i}{m_2}\binom{m_1-1}{m_2-1}}{\binom{N_i+m_1-1}{N_i-1}}, \quad m_2 \leqslant N_i. \tag{14}$$

In this case, $m_2$ (macro)pixels are exposed by the field and the probability of $c_i$ detections ($c_i \leqslant m_2$) is given by the matrix $K^{i,\infty}(c_i,m_2)$ written in Eq. (10), i.e., as if there is an infinite number of (macro)pixels in the camera. The matrix $G^{i,N_i}(c_i,n_i)$ then takes its final approximative form:

$$G^{i,N_i}(c_i,n_i) = \sum_{m_2=0}^{\min(m_1,N_i)} \sum_{m_1=0}^{n_i} K^{i,\infty}(c_i,m_2) \times \gamma^{i,N_i}(m_2,m_1) K_0(m_1,n_i), \tag{15}$$

where the matrix $K_0$ is defined in Eq. (13).

It has been assumed in the derivation of Eq. (15) that each of the exposed $m_2$ (macro)pixels contains only one photon (see the limit $N \to \infty$). This approximation can be improved. If $m_1$ photons are registered at $m_2$ (macro)pixels, an average photon number occurring in one (macro)pixel is $m_1/m_2$. The average photon number $m_1/m_2$ greater than 1 leads to a higher probability of detection. This increase of detection probability can be modeled by an effective increase of detection quantum efficiency (see Appendix). The improved matrix $G^{i,N_i}(c_i,n_i)$ can then be determined along the relation

$$G^{i,N_i}(c_i,n_i) = \sum_{m=0}^{n_i} \Gamma^{i,N_i}(c_i,m) K_0(m,n_i) \tag{16}$$

and

$$\Gamma^{i,N_i}(c_i,m) = \sum_{m_2=1}^{\min(m,N_i)} \sum_{l=0}^{\min(c_i,m_2)} \binom{m_2}{l} \left[1-\exp\left(-\eta_i \frac{m}{m_2}\right)\right]^l \left[\exp\left(-\eta_i \frac{m}{m_2}\right)\right]^{m_2-l} \frac{D_i^{c_i-l}}{(c_i-l)!} \exp(-D_i) \frac{\binom{N_i}{m_2}\binom{m-1}{m_2-1}}{\binom{N_i+m-1}{N_i-1}}. \tag{17}$$

On the other hand, weak detected fields allow the following simplification. If the maximum number $c_i$ of counts is much less than the number $N_i$ of (macro)pixels the expression for matrix $K^{i,N_i}$ in Eq. (9) can be successfully approximated using the relation $(1+x)^{n_i} \approx \exp(xn_i)$ for $|x| \ll 1$. We then arrive at the matrix $G^{i,N_i}(c_i,n_i)$ in the form

$$G^{i,N_i}(c_i,n_i) = \sum_{m=0}^{n_i} K_{\rm exp}^{i,N_i}(c_i,m) K_0(m,n_i) \tag{18}$$

and

$$K_{\rm exp}^{i,N_i}(c_i,m) = \binom{N_i}{c_i} (1-d_i)^{N_i-c_i} (1-\eta_i)^{m-c_i} \times \left[d_i(1-\eta_i) + \eta_i \frac{m}{N_i}\right]^{c_i}. \tag{19}$$

The expression in Eq. (19) has a simple interpretation: $m-c_i$ impinging photons are not registered with probability $1-\eta_i$ per photon. There occur $c_i$ counts given either by impinging photons with probability $m\eta_i/N_i$ per photon or by dark counts with probability $d_i(1-\eta_i)$. $N_i - c_i$ (macro)pixels cannot feel dark counts with probability $1-d_i$ per (macro)pixel.

## IV. INHOMOGENEOUS TRANSVERSE INTENSITY PROFILE OF A DETECTED BEAM

If the intensity transverse profile of a beam impinging on an iCCD camera is inhomogeneous, we can divide (macro)pixels of the camera into $M_i$ groups assuming the same level of illumination of (macro)pixels belonging to one group. A $j$th group of (macro)pixels is characterized by probability $\tau_{i_j}$ that a photon present in beam $i$ ($i = S,I$) impinges on one (macro)pixel from this group, by the number $\nu_{i_j}$ of (macro)pixels, by the quantum detection efficiency $\eta_{i_j}$, by the dark-count rate $d_{i_j}$, and by the mean number $\mu_{i_j}$ of photons impinging on one (macro)pixel. It holds that $\sum_{j=1}^{M_i} \tau_{i_j}\nu_{i_j} = \eta_i$ and $\sum_{j=1}^{M_i} \nu_{i_j} = N_i$. The probability $\tau_{i_j}$ that a photon reaches one (macro)pixel of the $j$th group is linearly proportional to the mean number $\mu_{i_j}$ of photons coming to this (macro)pixel and can be expressed as

$$\tau_{i_j} = \frac{\mu_{i_j}}{\mu_i^{\rm av} N_i}, \quad i = S,I. \tag{20}$$

The average mean photon number $\mu_i^{\rm av}$ is given as $\mu_i^{\rm av} = \sum_{j=1}^{M_i} \mu_{i_j}\nu_{i_j}/N_i$.

A transformation matrix $\tilde{K}^{i,N_i}(c_i,n_i)$ that generalizes the matrix $K^{i,N_i}$ occurring in Eq. (9) and determines the

probability of $c_i$ counts caused by $n_i$ photons coming to the camera is given by the following $M_i$-dimensional convolution of matrices $K^{i,\nu_{ij}}$ written in Eq. (9) and characterizing the detection in the $j$th group of (macro)pixels:

$$\tilde{K}^{i,N_i}(c_i,n_i) = \left\{\left[\prod_{j=1}^{M_i}\sum_{n_j=0}^{n_i}\right]\Bigg|_{\sum_{j=1}^{M_i} n_j=n_i}\right\}\left\{\left[\prod_{j=1}^{M_i}\sum_{c_j=0}^{c_i}\right]\Bigg|_{\sum_{j=1}^{M_i} c_j=c_i}\right\} n_i!\prod_{j=1}^{M_i}\frac{\left(\tau_{i_j}\nu_{i_j}\right)^{n_j}}{n_j!}K^{i,\nu_{i_j}}(c_j,n_j), \quad i=S,I. \tag{21}$$

The matrix $\tilde{K}^{i,N_i}$ occurring in Eq. (21) can be rewritten into the following form if the matrices $K^{i,\nu_{i_j}}$ are expressed using the relation in Eq. (9):

$$\begin{aligned}\tilde{K}^{i,N_i}(c_i,n_i) = {} & \left\{\left[\prod_{j=1}^{M_i}\sum_{c_j=0}^{c_i}\right]\Bigg|_{\sum_{j=1}^{M_i} c_j=c_i}\right\}\left[\prod_{k=1}^{M_i}\binom{\nu_{i_k}}{c_k}\left(1-d_{i_k}\right)^{\nu_{i_k}}\right]\left\{\prod_{j=1}^{M_i}\sum_{l_j=0}^{c_j}\right\}\left[\prod_{k=1}^{M_i}\binom{c_k}{l_k}\frac{(-1)^{l_k}}{\left(1-d_{i_k}\right)^{l_k}}\right] \\ & \times(-1)^{c_i}\left[1-\sum_{k=1}^{M_i}\left(\tau_{i_k}\nu_{i_k}\eta_{i_k}\right)+\sum_{k=1}^{M_i}\left(l_k\tau_{i_k}\eta_{i_k}\right)\right]^{n_i}.\end{aligned} \tag{22}$$

If the number of (macro)pixels is sufficiently large compared to the number of impinging photons, consideration of the following limit is useful. In this limit, $\nu_{i_j}\to\infty$ for $j=1,\ldots,M_i$, assuming $\nu_{i_j}\tau_{i_j}$ [probability that a photon is detected in the $j$th group of (macro)pixels] to be constant. Also $d_{i_j}\nu_{i_j}=D_{i_j}$ [overall dark-count rate of all (macro)pixels in the $j$th group] is assumed to be constant. Then the expression in Eq. (22) simplifies and leaves the matrix $\tilde{K}^{i,N_i}$ in the form

$$\begin{aligned}\tilde{K}^{i,\infty}(c_i,n_i) = {} & \left\{\left[\prod_{j=1}^{M_i}\sum_{c_j=0}^{c_i}\right]\Bigg|_{\sum_{j=1}^{M_i} c_j=c_i}\right\}\left\{\prod_{j=1}^{M_i}\sum_{l_j=0}^{\min(c_j,n_i)}\right\}\frac{n_i!}{\left[\prod_{k=1}^{M_i} l_k!\right]\left(n_i-\sum_{k=1}^{M_i} l_k\right)!}\left[\prod_{k=1}^{M_i}\left(\tau_{i_k}\nu_{i_k}\eta_{i_k}\right)^{l_k}\right] \\ & \times\left[\prod_{k=1}^{M_i}\frac{D_{i_k}^{c_k-l_k}}{(c_k-l_k)!}\exp(-D_{i_k})\right]\left[1-\sum_{k=1}^{M_i}\left(\tau_{i_k}\nu_{i_k}\eta_{i_k}\right)\right]^{n_i-\sum_{k=1}^{M_i} l_k}, \quad i=S,I.\end{aligned} \tag{23}$$

The expression in Eq. (23) has a simple interpretation: $n_i$ photons impinging on the camera generate $l_j$ counts in a $j$th group of (macro)pixels with probability $\tau_{i_j}\nu_{i_j}\eta_{i_j}$ per photon and $(c_j-l_j)$ counts come from dark counts occurring in the $j$th group of (macro)pixels. The remaining $n_i-\sum_{k=1}^{M_i} l_k$ photons are not registered with probability $1-\sum_{j=1}^{M_i}(\tau_{i_j}\nu_{i_j}\eta_{i_j})$ per photon.

Provided that the maximum number of counts $c_j$ in a $j$th group of (macro)pixels is much less than the number of (macro)pixels $\nu_{i_j}$ in this group the approximate relation $(1+x)^{n_i}\approx\exp(n_i x)$ for $|x|\ll 1$ enables to rearrange the formula in Eq. (22) as follows:

$$\begin{aligned}&\tilde{K}_{\exp}^{i,N_i}(c_i,n_i) \\ &= \left\{\left[\prod_{j=1}^{M_i}\sum_{c_j=0}^{c_i}\right]\Bigg|_{\sum_{j=1}^{M_i} c_j=c_i}\right\}\left(1-\sum_{k=1}^{M_i}\left(\tau_{i_k}\nu_{i_k}\eta_{i_k}\right)\right)^{n_i-c_i}\left\{\prod_{j=1}^{M_i}\binom{\nu_{i_j}}{c_j}\left(1-d_{i_j}\right)^{\nu_{i_j}-c_j}\left(d_{i_j}\left[1-\sum_{k=1}^{M_i}\left(\tau_{i_k}\nu_{i_k}\eta_{i_k}\right)\right]+n_i\tau_{i_j}\eta_{i_j}\right)^{c_j}\right\}.\end{aligned} \tag{24}$$

The expression in Eq. (24) can be interpreted similarly as the formula in Eq. (19). If $c_i$ counts occur after $n_i$ photons enter the camera, $n_i-c_i$ photons are not registered with probability $1-\sum_{k=1}^{M_i}\tau_{i_k}\nu_{i_k}\eta_{i_k}$ per photon. In a $j$th group of (macro)pixels, $\nu_{i_j}-c_j$ (macro)pixels do not count a photon with probability $1-d_{i_j}$ per (macro)pixel (dark counts have to be "eliminated"). Finally $c_j$ (macro)pixels detect a photon either due to a successful registration of a photon taken from $n_i$ incident photons with probability $\tau_{i_j}\eta_{i_j}$ per photon or owing to a dark count with probability $d_{i_j}(1-\sum_{k=1}^{M_i}\tau_{i_k}\nu_{i_k}\eta_{i_k})$ (a dark count occurs if there is no detection caused by an impinging photon).

If the number $c_i$ of counts registered by an iCCD camera is low and the number of groups of (macro)pixels is greater, a useful alternative expression for the transfer matrix $\tilde{K}^{i,N_i}(c_i,n_i)$ given in Eq. (21) can be derived directly from Eq. (6) ($T_i=1$ and $R_i=0$ are assumed, $i=S,I$):

$$\tilde{K}^{i,N_i}(c_i,n_i) = \left\{\left[\prod_{j=1}^{M_i}\sum_{c_j=0}^{c_i}\right]\Bigg|_{\sum_{j=1}^{M_i} c_j=c_i}\right\}\tilde{K}_{i,\{c_1,\ldots,c_{M_i}\}}(c_i,n_i), \quad i=S,I, \tag{25}$$

where the coefficient $\tilde{K}_{i,\{c_1,\ldots,c_{M_i}\}}(c_i,n_i)$ gives the probability that $c_j$ counts have occurred in the $j$th group of (macro)pixels; $\sum_{j=1}^{M_i} c_j = c_i$. It can be expressed as follows:

$$\tilde{K}_{i,\{c_1,\ldots,c_{M_i}\}}(c_i,n_i) = \left[\prod_{j=1}^{M_i}\binom{\nu_{i_j}}{c_j}\left(1-d_{i_j}\right)^{\nu_{i_j}}\right]\left\{(-1)^{c_i}\Theta_i^{n_i} + (-1)^{c_i-1}\sum_{k_1=1}^{c_i}\frac{\left[\Theta_i+\tau_{i\sigma_i(k_1)}\eta_{i\sigma_i(k_1)}\right]^{n_i}}{1-d_{i\sigma_i(k_1)}}\right.$$
$$+(-1)^{c_i-2}\sum_{k_1=1}^{c_i-1}\sum_{k_2=k_1+1}^{c_i}\frac{\left[\Theta_i+\tau_{i\sigma_i(k_1)}\eta_{i\sigma_i(k_1)}+\tau_{i\sigma_i(k_2)}\eta_{i\sigma_i(k_2)}\right]^{n_i}}{\left(1-d_{i\sigma_i(k_1)}\right)\left(1-d_{i\sigma_i(k_2)}\right)}$$
$$\left.+(-1)^{c_i-3}\sum_{k_1=1}^{c_i-2}\sum_{k_2=k_1+1}^{c_i-1}\sum_{k_3=k_2+1}^{c_i}\frac{\left[\Theta_i+\sum_{m=1}^{3}\left(\tau_{i\sigma_i(k_m)}\eta_{i\sigma_i(k_m)}\right)\right]^{n_i}}{\prod_{m=1}^{3}\left(1-d_{i\sigma_i(k_m)}\right)}+\cdots+\frac{\left[\Theta_i+\sum_{m=1}^{c_i}\left(\tau_{i\sigma_i(k_m)}\eta_{i\sigma_i(k_m)}\right)\right]^{n_i}}{\prod_{m=1}^{c_i}\left(1-d_{i\sigma_i(k_m)}\right)}\right\}. \tag{26}$$

The symbol $\Theta_i$ introduced in Eq. (26) denotes the probability that a photon is not registered by the camera; i.e.,

$$\Theta_i = 1-\sum_{j=1}^{M_i}\left(\tau_{i_j}\nu_{i_j}\eta_{i_j}\right), \qquad i=S,I. \tag{27}$$

The vector $\sigma_i$ in Eq. (26) is composed of $c_i$ elements ($i=S,I$); its $j$th element gives the number of group of (macro)pixels that registered the $j$th click ($j=1,\ldots,c_i$). Thus, the first $c_1$ elements equal 1, the next $c_2$ elements equal 2, and so on.

## V. RECONSTRUCTION OF THE JOINT SIGNAL-IDLER PHOTON-NUMBER DISTRIBUTION

The probabilities (frequencies) $f(c_S,c_I)$ are measured in the experiment and the relation in Eq. (11) has to be inverted in order to obtain the joint signal-idler photon-number distribution $p(n_S,n_I)$ beyond the nonlinear crystal. The relation in Eq. (11) together with the coefficients $G^{i,N_i}(c_i,n_i)$ defined in Eq. (12) can be inverted under special conditions analytically. For instance, if $D_S = D_I = 0$ the inversion relation is found using the "convolution" of function $f$ with the Bernoulli distributions with efficiencies $1/(T_S\eta_S)$ and $1/(T_I\eta_I)$ that are greater than 1. For more general cases, a method of direct matrix inversion has been elaborated [44,45]. However, analytical approaches are not suitable for processing real experimental data [46] because of numerical instabilities and the occurrence of artifacts. On the other hand, reconstruction algorithms have been found to be suitable for this task [21]. Such algorithms are able to find a reconstructed joint signal-idler photon-number distribution $\rho_{\mathrm{rec}}(n_S,n_I)$ that matches the measured frequencies $f(c_S,c_I)$ in the best way with respect to a given criterion. Here, we consider the Kullback-Leibler divergence as a measure of the distance between the experimental data and data provided by the developed theory. The reconstructed joint signal-idler photon-number distribution $\rho_{\mathrm{rec}}(n_S,n_I)$ minimizing the Kullback-Leibler divergence can then be found as a steady point of an iteration algorithm [47,48]:

$$\rho^{(n+1)}(n_S,n_I) = \rho^{(n)}(n_S,n_I)\sum_{i_S,i_I=0}^{\infty}\frac{f(i_S,i_I)G^{S,N_S}(i_S,n_S)G^{I,N_I}(i_I,n_I)}{\sum_{j_S,j_I=0}^{\infty}G^{S,N_S}(i_S,j_S)G^{I,N_I}(i_I,j_I)\rho^{(n)}(j_S,j_I)}. \tag{28}$$

The symbol $\rho^{(n)}(n_S,n_I)$ denotes a joint signal-idler photon-number distribution after an $n$th step of the iteration, and $\rho^{(0)}(n_S,n_I)$ is an arbitrary initial photon-number distribution. We note that each element of the initial photon-number distribution has to be nonzero in order to be considered in the iteration process.

Convergence of the iteration process can be monitored using parameter $S$ that gives the declination of the reconstructed photon-number distribution from the measured frequencies $f(c_S,c_I)$ and is determined along the formula

$$S^{(n)} = \left[\sum_{c_S,c_I=0}^{\infty}\left|f(c_S,c_I)-\sum_{j_S,j_I=0}^{\infty}G^{S,N_S}(c_S,j_S)G^{I,N_I}(c_I,j_I)\rho^{(n)}(j_S,j_I)\right|^2\right]^{1/2}. \tag{29}$$

Alternatively, also covariance $C$ of the signal and idler photon numbers, $n_S$ and $n_I$, derived for the joint photon-number distribution $\rho$,

$$C^{(n)} = \frac{\langle\Delta n_S\Delta n_I\rangle}{\sqrt{\langle(\Delta n_S)^2\rangle\langle(\Delta n_I)^2\rangle}}, \quad \Delta n_i = n_i-\langle n_i\rangle, \quad i=S,I,$$
$$\left\langle n_S^k n_I^l\right\rangle = \sum_{n_S=0}^{\infty}\sum_{n_I=0}^{\infty}n_S^k n_I^l\rho^{(n)}(n_S,n_I), \quad k,l=0,1,\ldots, \tag{30}$$

can be used as a useful indicator. The reason is that the initial photon-number distribution $\rho^{(0)}$ is usually considered without any correlation and the iteration process gradually reveals photon-number correlations present in the joint signal-idler field. We note that we have checked by numerical simulations that the reconstruction algorithm cannot reveal correlations provided that the measured frequencies $f(c_S,c_I)$ describe two independent fields.

Here, we analyze three photon-number distributions obtained under different conditions using the experimental setup shown in Fig. 2. Photon pairs are generated in a 5-mm-long beta barium borate (BBO) crystal cut for a type I process ($\theta = 50°, \phi = 90°$) pumped by ultrashort pulses delivered by a cavity-dumped titanium-sapphire femtosecond laser at a wavelength of 840 nm followed by a third-harmonic generator. The pulses at the fundamental wavelength are about 150 fs long. The laser system runs at a repetition rate of 50 kHz and, after converting the 840-nm beam to its third harmonic, it typically delivers pulses with energy up to 45 nJ. Degenerate signal and idler photons occur at the cone layer behind the crystal and leave the crystal at the outer output half-angle of 13°. Photons in the idler field are reflected from a high-reflectivity mirror (>99% at 560 nm) and impinge on an intensified CCD camera (Andor iStar 734). The camera has 1 megapixel resolution with $13 \times 13\ \mu\text{m}^2$ pixels but we use $8 \times 8$ hardware binning to increase the readout rate. The detection events are processed using our own software employing thresholding, event centroid finding, and photon counting. The software is optimized to achieve maximum detection efficiency, which we evaluate to 23% near the degenerate wavelength of 560 nm. Three regions of interest are defined in the field of view of the camera: the first one is for the signal field, the second one is for the idler field, and the last region serves for reference measurements of the noise level. The whole field of the camera is filtered by a high-transmittance high-pass filter blocking light below 490 nm and an interference filter of 14 nm FWHM centered at 560 nm. The interference filter selects nearly frequency degenerate photon pairs. Since a single run of data acquisition usually takes several hours, the laser intensity is actively stabilized (the intensity noise lays below 0.3% rms) using a feedback loop and polarization attenuator. The intensifier of the camera is synchronously gated (gate duration equals 5 ns) by cavity-dumper trigger pulses to minimize the noise from the laboratory.

In the experimental setup, histograms $f(c_S,c_I)$ of photoelectron numbers have been taken under two different intensity conditions. In the first case (a), the measurement has been performed for the lowest signal and idler intensities allowed by the setup. The limiting intensities are given by the noise of the camera and stray light from the laboratory. The second case (b) represents a typical result obtained under most suitable conditions. The third case (c) corresponds to the measurement done with greater signal and idler intensities and the histogram $f(c_S,c_I)$ has been obtained by summing up five neighbor frames together. We thus have three representative data sets with mean photoelectron numbers equal to 1.2, 8.6, and 43. The corresponding histograms $f(c_S,c_I)$ are shown in Fig. 3. Covariances of the photoelectron numbers $c_S$ and $c_I$ described by the histograms $f(c_S,c_I)$ plotted in Fig. 3 are in turn 23.8%, 21.4%, and 21.1%. This corresponds to the expected overall

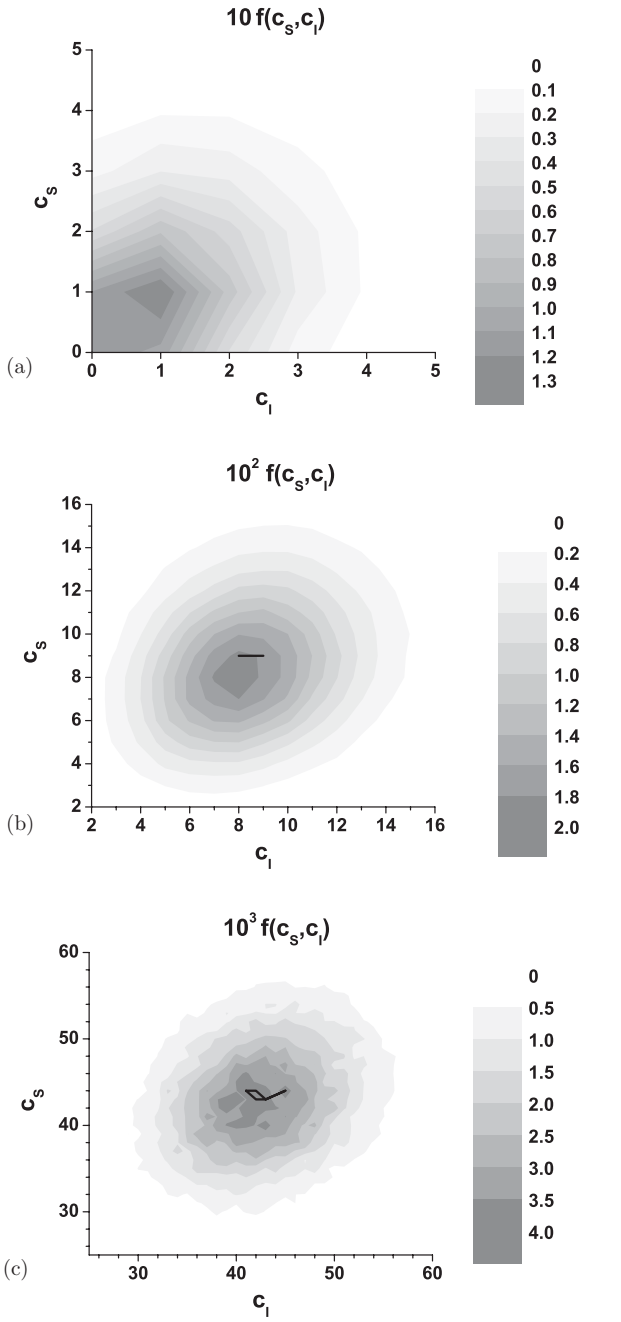


FIG. 3. Topological graphs of the measured histograms $f$ of signal ($c_S$) and idler ($c_I$) photoelectron numbers for three data sets denoted as (a), (b), and (c). A black curve encircles the area in which the classical inequality (31) is violated.

detection efficiencies $T_S\eta_S$ and $T_I\eta_I$ around 20% and the low level of single-photon noise.

In order to apply the iteration reconstruction algorithm described in Eq. (28) we need to know the overall detection efficiencies $T_S\eta_S$ and $T_I\eta_I$. In principle, they can be determined by knowing parameters of the experimental setup. However, the fragility of the experimental alignment enforces the determination from the obtained experimental data. The values of detection efficiencies can be derived either from the measured covariance between the signal and idler photoelectron numbers $c_S$ and $c_I$ or alternatively by applying

a method described in Sec. VI below that relies on finding the best fit to the experimental data. This method applied to data set (b) has provided $T_S\eta_S = 0.207$ and $T_I\eta_I = 0.205$, which have been used in the reconstruction. These values take into account the quantum detection efficiency of the iCCD camera as well as losses occurring in the setup (frequency filters, reflection on the output plane of the crystal and mirror). The reconstruction algorithm also needs the level of dark noise that has been monitored in the third region of interest of the photocathode; (a) $D_S = D_I = 0.03$, (b) 0.09, and (c) 0.46. The application of the formula in Eq. (28) has then resulted in the joint signal-idler photon-number distributions $p_{\rm rec}(n_S,n_I) \equiv \rho^{(\infty)}(n_S,n_I)$ appropriate for the output plane of the crystal and shown in Fig. 4. The initial joint signal-idler

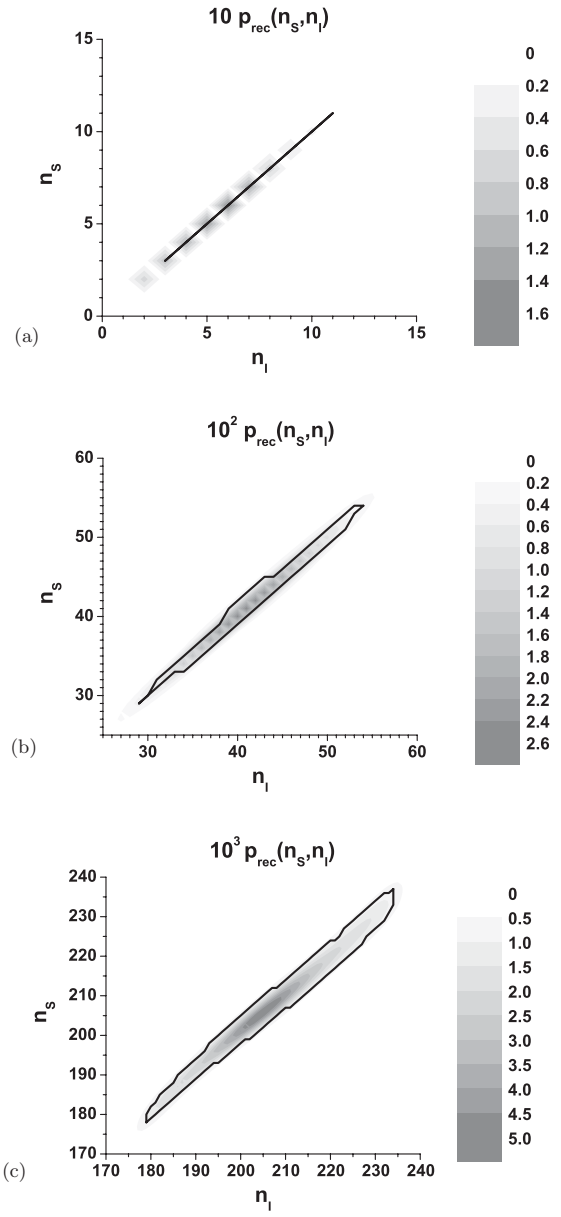


FIG. 4. Topological graphs of the reconstructed joint signal-idler photon-number distributions $p_{\rm rec}(n_S,n_I)$ for data sets (a), (b), and (c). A black curve encircles the area in which the classical inequality (31) is violated.

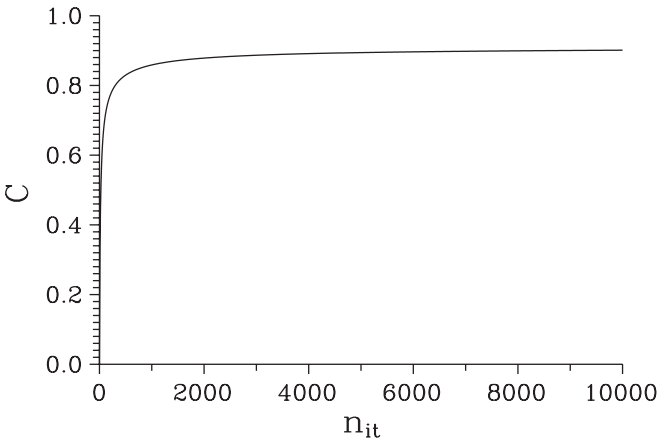


FIG. 5. Covariance $C$ of the signal and idler photon numbers $n_S$ and $n_I$ as it depends on the number $n_{\rm it}$ of the iteration step for data set (b).

photon-number distribution $\rho^{(0)}$ has been taken as uniform in all three cases. Covariances of the reconstructed joint signal-idler photon-number distributions $p_{\rm rec}$ equal (a) 90.0%, (b) 90.1%, and (c) 89.7%. These numbers show the ability of the reconstruction algorithm to recover paired correlations that have been weakened during the propagation and detection process. The fact that the obtained covariances do not approach 100% has two reasons: (1) there is an imperfect description of all noises occurring in the experiment, and (2) numerical implementation of the iteration reconstruction algorithm loses its precision with the increasing number of steps [29]. Both values of the parameter $S$ given in Eq. (29) and covariance $C$ defined in Eq. (30) can be used for monitoring convergence of the iteration process. Covariance $C$ has been found to be more sensitive. Typically several hundreds of iteration steps are needed to arrive at solid (asymptotic) results as documented in Fig. 5 valid for data set (b). In all three cases, 10 000 iteration steps have been applied.

The reconstructed joint signal-idler photon-number distributions $p_{\rm rec}$ show that the emitted fields are mainly composed of photon pairs that are responsible for nonzero covariances of the signal and idler photon numbers. Such fields are nonclassical in the sense that they cannot be described by non-negative Glauber-Sudarshan quasidistributions [37]. As a consequence, there even exist elements $p_{\rm rec}(n_S,n_I)$ of the joint photon-number distribution $p_{\rm rec}$ that violate the classical inequality [49]

$$p_{\rm rec}(n_S,n_I) \leqslant \frac{\langle n_S\rangle^{n_S}\langle n_I\rangle^{n_I}}{n_S!\,n_I!}\exp[-\langle n_S\rangle - \langle n_I\rangle]. \qquad (31)$$

However, nonclassical properties manifest also in quantities which determination is based on all elements of the joint photon-number distribution $p_{\rm rec}$.

### A. Important nonclassical characteristics of paired fields

Correlations in the signal and idler photon numbers $n_S$ and $n_I$ lead to narrowing of the distribution $p_-$ of the photon-number difference $n_S - n_I$ together with broadening of the distribution $p_+$ of the photon-number sum $n_S + n_I$. The

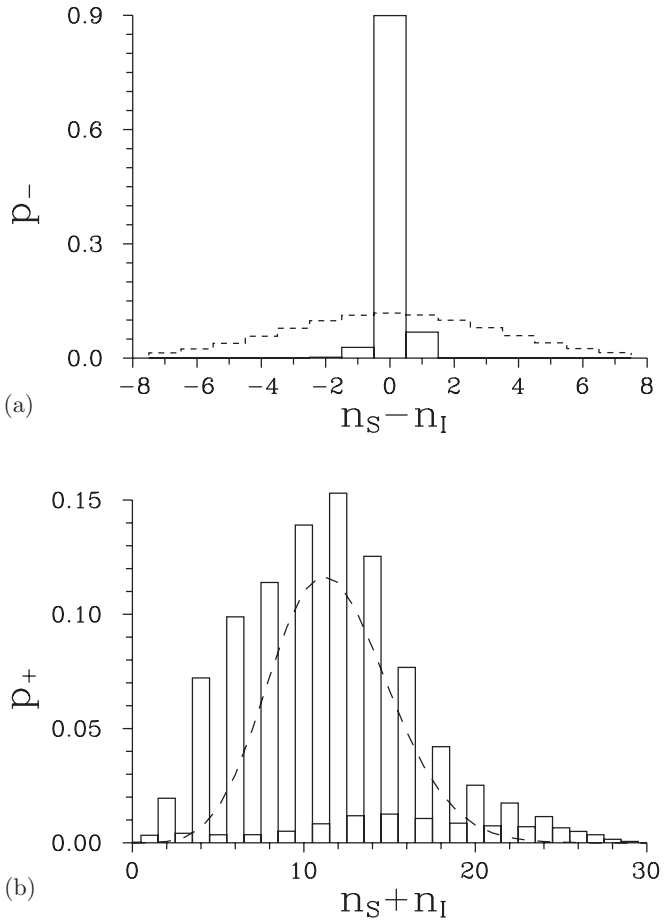


FIG. 6. (a) Distributions $p_-$ of the photon-number difference $n_S - n_I$ and (b) distributions $p_+$ of the photon-number sum $n_S + n_I$ for data set (b) (solid curves). Dashed curves give the distributions derived from the joint signal-idler photon-number distribution given as a direct product of the marginal signal and idler distributions; they are plotted for comparison.

distributions $p_+$ and $p_-$ are defined as

$$p_\pm(n) = \sum_{n_S=0}^{\infty} \sum_{n_I=0}^{\infty} \delta_{n,n_S \pm n_I}\, p_{\mathrm{rec}}(n_S, n_I). \tag{32}$$

The symbol $\delta$ is Kronecker's delta.

Fluctuations described by the distribution $p_-$ of the photon-number difference can even be lower than those corresponding to any classical field with no correlations [see Fig. 6(a)]. We then speak about sub-shot-noise correlations that can be quantified by parameter $R$ ($R < 1$ for nonclassical states):

$$R = \frac{\langle [\Delta(n_S - n_I)]^2 \rangle}{\langle n_S \rangle + \langle n_I \rangle}. \tag{33}$$

Considering the experimental data, we obtain (a) $R = 0.133$ (8.7 dB), (b) $R = 0.111$ (9.5 dB), and (c) $R = 0.117$ (9.3 dB). This means that all three detected fields are strongly nonclassical. We note that the discussed narrowing can also be observed for stronger fields utilizing correlations of photocurrents from two detectors [31].

On the other hand, the distribution $p_+$ of the photon-number sum is super-Poissonian; i.e., its Fano factor $F$ is greater than 1 [$F = \langle (\Delta n)^2 \rangle / \langle n \rangle$]. The suppression of its elements giving the probabilities of odd photon numbers represents its most striking feature [44]. If the field were composed only of photon pairs, these elements would have been zero. However, the presence of noise photons conceals this feature and so we can observe it only for the data set (a) obtained under low illumination [see Fig. 6(b)].

### B. Determination of photon-number statistics, measurement of intense fields, and role of the intensity profile

The type of statistics of the emitted photon pairs is an important characteristic [1,37]. According to the theory, if the emission occurs in one spatiotemporal mode, the photon-number statistics is Gaussian (thermal). However, the emission is usually observed in more than one independent spatiotemporal mode [45] and, as a consequence, the statistics of photon pairs declines toward a Poissonian distribution. The greater the number of modes, the closer the actual statistics to the Poissonian distribution. In the experiment the situation is more complex because of noises superimposed on the emitted paired field. The theory presented in Sec. VI below allows in principle to determine the number of paired modes and to extract the statistics of photon pairs. When the reconstruction algorithm is applied, we can only determine the statistics of marginal signal and idler fields and deduce the type of statistics of photon pairs from them. We note that a Fano factor $F$ is commonly used to judge the type of statistics or, more precisely, the declination of statistics from the Poissonian one.

The Fano factor is also extraordinarily important for the quantification of the effect of the presence of more than one photon in the area of one macropixel at the photocathode. If the probability of having more than one photon at one macropixel is non-negligible, the statistics of photoelectron numbers [$f(c_S, c_I)$] decline from photon-number statistics [$p_{\mathrm{rec}}(n_S, n_I)$]. The fact that one macropixel cannot resolve photon numbers leads to a systematic decrease of the Fano factor of a detected field. The stronger the field the smaller the value of the Fano factor. This effect is in its nature the same as a dead-time effect in time-resolved detection. However, this effect can be corrected using appropriate transfer matrices. When stronger fields are measured, the transfer matrices $K^S$ and $K^I$ should even be corrected with respect to the field intensity profile as suggested in Sec. IV.

Data set (c) has been obtained in the discussed regime and the regions of interest were composed of $N_S = N_I = 6528$ macropixels. Here, the Fano factors of the marginal distributions of detected photoelectrons are $F_S = 0.996$ and $F_I = 1.008$. We can see in Fig. 7 how the Fano factors $F_S$ and $F_I$ of the marginal distributions derived from the reconstructed joint signal-idler photon-number distribution $p_{\mathrm{rec}}$ depend on the form of transformation matrices $K^{S,N_S}$ and $K^{I,N_I}$, in more detail on parameter $M$ ($M = M_S = M_I$) giving the number of areas inside the detection region. In the $k$th area there are pixels illuminated by intensities greater than $(k-1)\Delta I$ and lower than $k\Delta I$, $k = 1, \ldots, M$ [$\Delta I = I_{\max}/M$, $I_{\max}$ being the maximum intensity found in the profile]. The Fano factors $F_S$ and $F_I$ plotted for $M = 0$ in Fig. 7 are obtained assuming the transfer matrices given in Eq. (10) [$N_S, N_I \to \infty$]. We can see from the curves in Fig. 7 that the more precise the form of transfer matrices the better the elimination of the effect and so the greater the values of Fano factors $F_S$ and $F_I$. We can

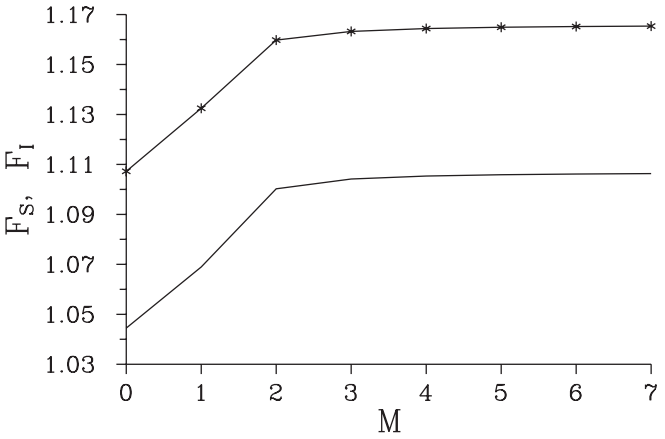


FIG. 7. Fano factors $F_S$ (solid curve) and $F_I$ (solid curve with $*$) of the marginal signal and idler photon-number distributions obtained from the reconstructed joint signal-idler photon-number distribution $p_{\mathrm{rec}}$ as they depend on the number $M$ of areas defined inside the detection region of interest.

also deduce that it is sufficient to divide the detection region of interest into several areas to arrive at reliable results. The reconstruction of fields described by data set (c) clearly demonstrates the ability of the method to cope with this problem.

The Fano factors of marginal distributions have been determined as (a) $F_S = 1.32$, (b) 1.126, and (c) 1.106 and (a) $F_I = 1.33$, (b) 1.126, and (c) 1.165. These values show that the observed down-conversion has been emitted into several tens or even hundreds of independent spatiotemporal modes.

Provided that the generated joint signal-idler field is multimode and the photons are preferably generated in the spontaneous process, we can assume that relative phases of different modes have random values. In this case, the joint signal-idler field can fully be characterized by a joint signal-idler quasi-distribution $P_W$ of signal and idler integrated intensities. The quasi-distribution $P_W$ can be uniquely derived from the joint signal-idler photon-number distribution $p_{\mathrm{rec}}$ using the decomposition into Laguerre polynomials [12,37]. Due to the pairwise character of the emitted fields, the joint signal-idler quasi-distributions $P_W$ of integrated intensities attain negative values in certain regions [50,51].

## VI. FIT OF THE EXPERIMENTAL DATA USING THE MODEL OF SIGNAL AND NOISE

An alternative approach for obtaining a joint signal-idler photon-number distribution in the output plane of the crystal can be developed assuming a certain form of this distribution. We can assume for physical reasons that the overall field can be described by a certain form of superposition of signal and noise and can also be decomposed into three independent contributions. The first contribution describes photon pairs that are inside $m_p$ independent modes with mean photon-pair numbers $b_p$. The second (third) contribution takes into account the presence of noise in the signal (idler) field and is composed of $m_S$ ($m_I$) independent modes with mean photon numbers $b_S$ ($b_I$).

On the experimental side of the problem there are five first- and second-order moments of the measured photoelectron numbers: $\langle c_S \rangle$, $\langle c_I \rangle$, $\langle c_S^2 \rangle$, $\langle c_I^2 \rangle$, and $\langle c_S c_I \rangle$. Moreover, a reliable determination of overall detection efficiencies $T_S\eta_S$ and $T_I\eta_I$ in the experimental setup is difficult. That is why we can consider the efficiencies $T_S\eta_S$ and $T_I\eta_I$ as parameters that should be determined from the experimental data. We thus have eight independent parameters and five measured quantities. The requirement of minimum entropy of the joint photoelectron distribution used for fitting the experimental data can be applied to find the most appropriate form of the joint signal-idler photon-number distribution $p$ (details can be found in a forthcoming publication).

The application of the method to data set (b) has provided the values $T_S\eta_S = 0.207$ and $T_I\eta_I = 0.205$ that were used in the reconstruction in Sec. V. Values of the remaining parameters have been found as $m_p = 628$, $b_p = 0.066$, $m_S = 0.46$, $b_S = 0.173$, $m_I = 0.018$, and $b_I = 2.32$. Comparison of the obtained joint signal-idler photon-number distribution $p_{\mathrm{fit}}$ with the distribution $p_{\mathrm{rec}}$ revealed by the reconstruction is given in Fig. 8. We can see that the distribution $p_{\mathrm{fit}}$ is

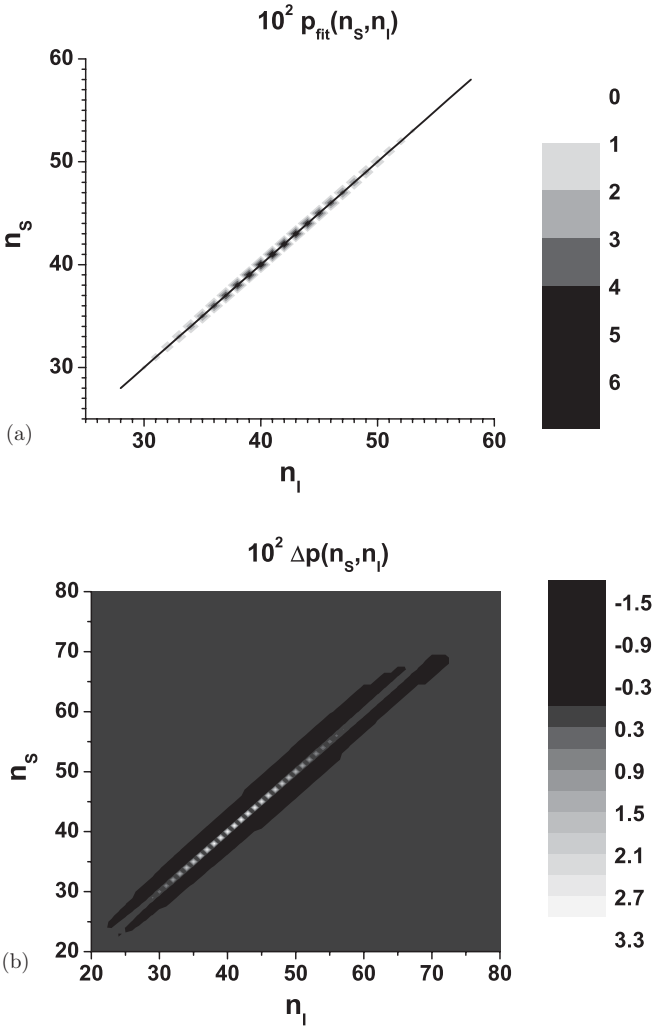


FIG. 8. Topological graphs of (a) joint signal-idler photon-number distribution $p_{\mathrm{fit}}(n_S,n_I)$ obtained by the fitting method and (b) difference $\Delta p(n_S,n_I)$ of photon-number distributions $p_{\mathrm{fit}}$ and $p_{\mathrm{rec}}$ obtained by the fitting and reconstruction methods, respectively $[\Delta p(n_S,n_I) = p_{\mathrm{fit}}(n_S,n_I) - p_{\mathrm{rec}}(n_S,n_I)]$ for data set (b). The black line identifies the elements $p_{\mathrm{fit}}(n_S,n_I)$ violating the classical inequality (31).

"narrower"; i.e., it contains less noise ($F_S = 1.066$, $F_I = 1.068$). This is in agreement with the expectation that the fitting method is by its nature more efficient in eliminating the noise. We note for comparison that using the fitting method covariance $C$ of the signal and idler photon numbers $n_S$ and $n_I$ equals 99.7% and $R = 0.028$. However, compared to the reconstruction method, the fitting method does not take into account the number of macropixels and also cannot be applied to more intense fields.

## VII. CONCLUSIONS

We have developed a method for the reconstruction of a joint signal-idler photon-number distribution using the measured histograms of photoelectron numbers and an iteration expectation maximization algorithm. In the framework of a general detection theory we have found formulas for the transfer matrices that give linear relations between elements of a photon-number distribution and the corresponding photoelectron distribution. These formulas take into account finite quantum detection efficiencies, the level of dark counts, as well as finite numbers of detection macropixels. Special formulas appropriate for very weak as well as high illumination intensities have been found. A method for the inclusion of a transverse intensity profile into the form of transfer matrices has been suggested. Three joint signal-idler photon-number distributions differing in mean photon numbers have been reconstructed using the developed method. Some of their elements violate a classical inequality. Fluctuations of the difference of signal and idler photon numbers are highly suppressed due to pairing of photons in all three cases (sub-shot-noise correlations). Moreover, there occurs a partial suppression of elements corresponding to odd photon numbers in the distribution of the sum of signal and idler photon numbers for the weakest measured field. The developed reconstruction method has been compared to a method that provides the best fit of the experimental data assuming a joint signal-idler photon-number distribution in the form of superposition of signal and noise. The power of the reconstruction method to eliminate noise has been found weaker on one side. On the other side, it allows a more realistic description of the detection process. This is invaluable for higher detector illumination intensities. We believe that the developed reconstruction method will stimulate a broader use of iCCD cameras as photon-number-resolving detectors.

## ACKNOWLEDGMENTS

The authors thank J. Peřina for helpful discussions. Support by Project No. 1M06002, No. COST OC 09026, and the Operational Program Research and Development for Innovations—European Regional Development Fund (Project No. CZ.1.05/2.1.00/03.0058) of the Ministry of Education of the Czech Republic as well as Project No. IAA100100713 of GA AV ČR is acknowledged.

## APPENDIX: DETERMINATION OF AN EFFECTIVE DETECTION QUANTUM EFFICIENCY

We assume that a Poissonian field with mean photon number $\mu$ and statistical operator $\hat{\varrho}$,

$$\hat{\varrho} = \sum_{n=0}^{\infty} \frac{\mu^n}{n!} \exp(-\mu) |n\rangle\langle n|, \tag{A1}$$

impinges on a detector with quantum efficiency $\eta$ and dark-count rate $d$. The probability $p^{\mathrm{Pois}}$ of registering a photon is given as

$$\begin{aligned} p^{\mathrm{Pois}} &= \mathrm{Tr}(\hat{D}\hat{\varrho}) \\ &= 1 - (1-d)\exp(-\eta\mu); \end{aligned} \tag{A2}$$

the detection operator $\hat{D}$ has been introduced in Eq. (3).

If there is just one photon in the Fock state ($\hat{\varrho} = |1\rangle\langle 1|$) in a detected field, the probability $p^{\mathrm{Fock}}$ of its counting is

$$p^{\mathrm{Fock}} = 1 - (1-d)(1-\eta). \tag{A3}$$

The requirement of equal detection probabilities $p^{\mathrm{Fock}}$ and $p^{\mathrm{Pois}}$ results in an effective quantum efficiency $\eta^{\mathrm{eff}}$ depending on $\mu$:

$$\eta^{\mathrm{eff}}(\mu) = 1 - \exp(-\eta\mu). \tag{A4}$$

[1] L. Mandel and E. Wolf, *Optical Coherence and Quantum Optics* (Cambridge University Press, Cambridge, 1995).
[2] D. F. Walls and G. J. Milburn, *Quantum Optics* (Springer, Berlin, 1995).
[3] J. Peřina, Z. Hradil, and B. Jurčo, *Quantum Optics and Fundamentals of Physics* (Kluwer, Dordrecht, 1994).
[4] D. Bouwmeester, J. W. Pan, K. Mattle, M. Eibl, H. Weinfurter, and A. Zeilinger, Nature (London) **390**, 575 (1997).
[5] A. Migdall, Phys. Today **52**, 41 (1999).
[6] G. Brida, I. P. Degiovanni, M. Genovese, M. L. Rastello, and I. R. Berchera, Opt. Express **18**, 20572 (2010).
[7] T. S. Larchuk, M. C. Teich, and B. E. A. Saleh, Ann. N. Y. Acad. Sci. **755**, 680 (1995).
[8] F. Paleari, A. Andreoni, G. Zambra, and M. Bondani, Opt. Express **12**, 2816 (2004).
[9] O. Jedrkiewicz, Y. K. Jiang, E. Brambilla, A. Gatti, M. Bache, L. A. Lugiato, and P. Di Trapani, Phys. Rev. Lett. **93**, 243601 (2004).
[10] A. Agliati, M. Bondani, A. Andreoni, G. De Cillis, and M. Paris, J. Opt. B: Quantum Semiclassical Opt. **7**, S652 (2005).
[11] O. Haderka, J. Peřina Jr., and M. Hamar, J. Opt. B: Quantum Semiclassical Opt. **7**, S572 (2005).
[12] O. Haderka, J. Peřina Jr., M. Hamar, and J. Peřina, Phys. Rev. A **71**, 033815 (2005).
[13] M. Bondani, A. Allevi, G. Zambra, M. G. A. Paris, and A. Andreoni, Phys. Rev. A **76**, 013833 (2007).
[14] J.-L. Blanchet, F. Devaux, L. Furfaro, and E. Lantz, Phys. Rev. Lett. **101**, 233604 (2008).
[15] G. Brida, L. Caspani, A. Gatti, M. Genovese, A. Meda, and I. R. Berchera, Phys. Rev. Lett. **102**, 213602 (2009).

[16] J. Kim, S. Takeuchi, Y. Yamamoto, and H. H. Hogue, Appl. Phys. Lett. **74**, 902 (1999).
[17] M. Ramilli, A. Allevi, V. Chmill, M. Bondani, M. Caccia, and A. Andreoni, J. Opt. Soc. Am. B **27**, 852 (2010).
[18] A. Allevi, M. Bondani, and A. Andreoni, Opt. Lett. **35**, 1707 (2010).
[19] A. J. Miller, S. W. Nam, J. M. Martinis, and A. V. Sergienko, Appl. Phys. Lett. **83**, 791 (2003).
[20] O. Haderka, M. Hamar, and J. Peřina Jr., Eur. Phys. J. D **28**, 149 (2004).
[21] J. Řeháček, Z. Hradil, O. Haderka, J. Peřina Jr., and M. Hamar, Phys. Rev. A **67**, 061801(R) (2003).
[22] D. Achilles, C. Silberhorn, C. Sliwa, K. Banaszek, and I. A. Walmsley, Opt. Lett. **28**, 2387 (2003).
[23] D. Achilles, C. Silberhorn, C. Sliwa, K. Banaszek, and I. A. Walmsley, J. Mod. Opt. **51**, 1499 (2004).
[24] M. J. Fitch, B. C. Jacobs, T. B. Pittman, and J. D. Franson, Phys. Rev. A **68**, 043814 (2003).
[25] M. J. Fitch, B. C. Jacobs, T. B. Pittman, and J. D. Franson, J. Mod. Opt. **51**, 1499 (2004).
[26] B. M. Jost, A. V. Sergienko, A. F. Abouraddy, B. E. A. Saleh, and M. C. Teich, Opt. Express **3**, 81 (1998).
[27] M. Hamar, J. Peřina Jr., O. Haderka, and V. Michálek, Phys. Rev. A **81**, 043827 (2010).
[28] G. Zambra, A. Andreoni, M. Bondani, M. Gramegna, M. Genovese, G. Brida, A. Rossi, and M. G. A. Paris, Phys. Rev. Lett. **95**, 063602 (2005).
[29] G. Zambra and M. G. A. Paris, Phys. Rev. A **74**, 063830 (2006).
[30] M. Vasilyev, S. K. Choi, P. Kumar, and G. Mauro D'Ariano, Phys. Rev. Lett. **84**, 2354 (2000).
[31] Y. Zhang, K. Kasai, and M. Watanabe, Opt. Lett. **27**, 1244 (2002).
[32] J. Peřina and J. Křepelka, J. Opt. B: Quantum Semiclassical Opt. **7**, 246 (2005).
[33] J. Peřina and J. Křepelka, J. Eur. Opt. Soc. Rapid Publ. **1**, 06002 (2006).
[34] J. Peřina and J. Křepelka, Opt. Commun. **265**, 632 (2006).
[35] J. Peřina and J. Křepelka, J. Phys. B **41**, 085501 (2008).
[36] J. Peřina and J. Křepelka, Eur. Phys. J. D **281**, 4705 (2008).
[37] J. Peřina, *Quantum Statistics of Linear and Nonlinear Optical Phenomena* (Kluwer, Dordrecht, 1991).
[38] J. Peřina Jr., O. Haderka, and J. Soubusta, Phys. Rev. A **64**, 052305 (2001).
[39] O. Haderka and J. Peřina Jr., in *Decoherence and Its Applications in Quantum Computation and Information Transfer,* edited by T. Gonis and P. E. A. Turchi, NATO Science Series, Series III: Computer and System Sciences Vol. 182 (IOP Press, Amsterdam, 2001), p. 186.
[40] O. Haderka and J. Peřina Jr., in *Wave and Quantum Aspects of Contemporary Optics,* edited by J. Peřina, M. Hrabovský, and J. Křepelka, Proc. SPIE, Vol. 4356 (SPIE, Bellingham, WA, 2001), p. 61.
[41] R. A. Campos, B. E. A. Saleh, and M. C. Teich, Phys. Rev. A **40**, 1371 (1989).
[42] P. Törmä, T. Kiss, I. Jex, and H. Paul, Jemna Mech. Opt. **11-12**, 338 (1996).
[43] S. Brattke, B. T. H. Varcoe, and H. Walther, Phys. Rev. Lett. **86**, 3534 (2001).
[44] E. Waks, E. Diamanti, B. C. Sanders, S. D. Bartlett, and Y. Yamamoto, Phys. Rev. Lett. **92**, 113602 (2004).
[45] M. Avenhaus, H. B. Coldenstrodt-Ronge, K. Laiho, W. Mauerer, I. A. Walmsley, and C. Silberhorn, Phys. Rev. Lett. **101**, 053601 (2008).
[46] D. Mogilevtsev, Z. Hradil, and J. Peřina, J. Mod. Opt. **44**, 2261 (1997).
[47] A. P. Dempster, N. M. Laird, and D. B. Rubin, J. R. Stat. Soc. B **39**, 1 (1977).
[48] Y. Vardi and D. Lee, J. R. Stat. Soc. B **55**, 569 (1993).
[49] M. Hillery, Phys. Rev. A **35**, 725 (1987).
[50] J. Peřina, J. Křepelka, J. Peřina Jr., M. Bondani, A. Allevi, and A. Andreoni, Eur. Phys. J. D **53**, 373 (2009).
[51] J. Peřina and J. Křepelka, Opt. Commun. **284**, 4941 (2011).